Identification of nuclear pore proteins at plasmodesmata

T. Moritz Schladt[1,2,*], Manuel Miras[1,2,8,*], Jona Obinna Ejike[1,2,*], Mathieu Pottier[1,2,9,*], Lin Xi[3], Andrea Restrepo-Escobar[1,2], Masayoshi Nakamura[4], Niklas Pütz[1,2], Sebastian Hänsch[2,5], Chen Gao[1,2], Julia Engelhorn[1,2], Marcel Dickmanns[1,2,6], Ahan Dalal[1,2], Sven Gombos[3], Ronja Lange[1,2], Rüdiger Simon[2,7], Waltraud X. Schulze[3] & Wolf B. Frommer[1,2,4,7,§]

[1] Heinrich Heine University Düsseldorf, Faculty of Mathematics and Natural Sciences, Institute for Molecular Physiology, Düsseldorf, Germany
[2] Cluster of Excellence on Plant Sciences, Heinrich Heine University Düsseldorf, Germany
[3] Department of Plant Systems Biology, University of Hohenheim, 70593 Stuttgart, Germany
[4] Institute for Transformative Biomolecules (WPI-ITbM), Nagoya University, Nagoya, Japan
[5] Center for Advanced Imaging; Heinrich Heine University Düsseldorf, Düsseldorf, Germany
[6] Department of Molecular Structural Biology, Max Planck Institute of Biochemistry, Martinsried, Germany
[7] Heinrich Heine University Düsseldorf, Faculty of Mathematics and Natural Sciences, Institute of Developmental Genetics, Germany
[8] New address: Department of Stress Biology and Plant Pathology, CEBAS-CSIC, Murcia, Spain
[9] New address: Université de Lorraine, INRAE, IAM, F-54000 Nancy, France

* Equal contribution
§ For correspondence: frommew@hhu.de

Abstract

Plasmodesmata (PD) exchange small molecules, RNAs and proteins between plant cells with an exclusion limit for passive, non-specific transport that varies with cell type, developmental and physiological states of the tissue. Moreover, PD facilitate the transport of specific cargo that may require chaperones or carriers to be transported. The precise mechanisms underlying PD transport are not entirely understood. Parallels between PD and the nuclear pore complex (NPC), which controls transport between nucleoplasm and cytoplasm, have been discussed previously. PD transport shares similar features with the phase separation dependent NPC transport. Here, bioinformatics, proteomics and imaging were used to identify proteins with similarities to phase separating nucleoporins (NUP). We identified 21 NUPs in PD fractions, and validated dual localization to NPC and PD for 6 NUPs. The transmembrane anchor NUP CPR5 localized to PD orifices as detected by high-resolution imaging. *cpr5* mutants had reduced intercellular transport activity for cargo larger than 54 kDa, but not for smaller cargo around 376 Da. The data indicates a role for NUP CPR5 in macromolecular transport through PD. Together this is consistent with the recruitment of NUPs in the green lineage to form a PD pore gating complex and is in line with the idea of a phase separation as diffusion barrier at PD.

INTRODUCTION

All kingdoms of life developed unique machineries for the direct intercellular exchange of small molecules, genetic information, and polypeptides: bacteria use pili, fungi use septa, metazoans developed gap junctions, and plants evolved the complex multimembrane plasmodesmata (PD) (*1–3*). PD are thought to mediate cell-to-cell sugar transport from source cells to the phloem, exchange metabolites between mesophyll and bundle sheath tissues in species that use C4 photosynthesis, translocate florigen from leaves to meristems, and perform many other functions (*4–6*). Despite their important role, their composition, structure, transport mechanism and regulation remain poorly understood.

RATIONALE

Some aspects of the transport of cargo through nuclear pore complexes (NPC) and PD, such as the types of cargo and the facilitation of transport for specific cargo, appear strikingly similar. We therefore hypothesized that PD may contain proteins with similar features as the ones constituting phase separation in the molecular barrier of the NPC [i.e., the phenylalanine–glycine nucleoporins (FG-NUPs)]. Such proteins may have arisen independently or may have evolved from the FG-NUPs. We used bioinformatics, proteomics and confocal imaging to identify potential candidate proteins for the transport channel of PD.

RESULTS

Nuclear pore proteins, in particular FG-NUPs as well as scaffold and transmembrane NUPs, constitute the functional gatekeepers of the NPC. FG-NUPs, scaffold NUPs and transmembrane NUPs were present in PD-enriched fractions and NUP fusions localized with PD markers. Topological studies revealed that the green lineage-specific membrane anchor NUP CPR5 is embedded into the ER membrane approaching the PD. High-resolution imaging showed that CPR5 localizes close to PD orifices. Analyses of passive passage of the heterologous green fluorescent protein (GFP) and of facilitated transport of the transcription factor SHORT-ROOT (SHR) indicated that intercellular exchange of polypeptides is partially impaired in *cpr5* mutants. The transport changes were specific for macromolecules, as no changes were detectable for the diffusion of a small molecule dye; indicating an involvement of NUPs in macromolecular cell-to-cell trafficking, similar to their role in nuclear-cytoplasmic transport.

CONCLUSION

Our results indicate the possibility that the green lineage recruited at least parts of the NPC to PD to generate a plasmodesmatal pore complex (PDPC). The presence of FG-NUPs at PD is in line with the idea of a phase separation as the permeability barrier in the PDPC. The overall PDPC structure must differ from the NPC due to the presence of a central desmotubule. It is well established that the NPC is highly flexible and can likely adopt diverse conformations due to the multivalent interaction network. Hence, deletion of the membrane anchor CPR5 could affect conformation of the PDPC and its associated permeability barrier and thereby restrict macromolecular trafficking. This work may open new ways to

understand the structure, function, transport mechanism and regulation of PD and how to engineer the permeability barrier between cells to alter plant properties.

Graphical Abstract

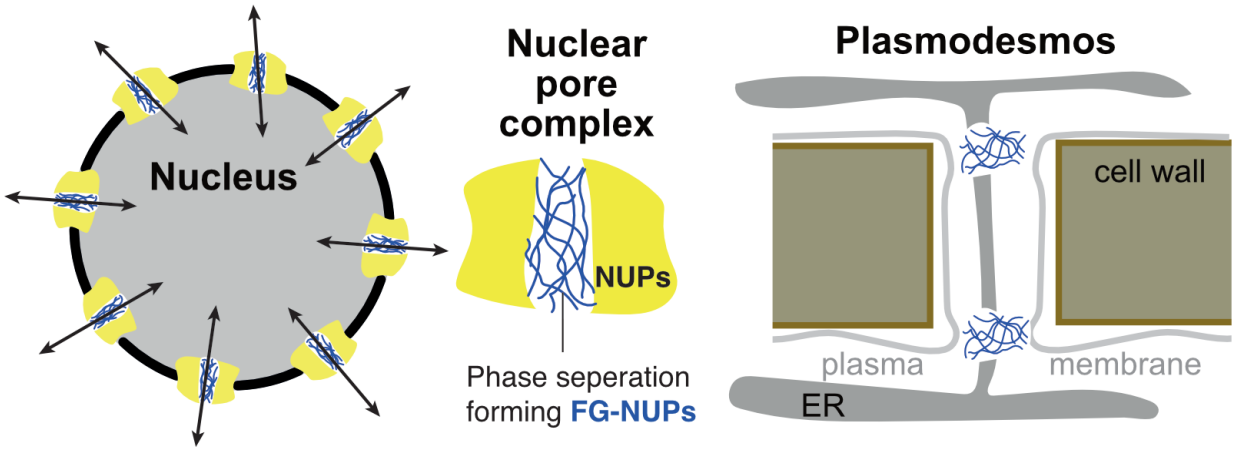

Left: nucleus with nuclear pore complexes (yellow) containing phase-separated domains generated by FG-NUPs (phenylalanine glycine- nuclear pore proteins). Middle: magnified nuclear pore complex. Right: Plasmodesmos embedded into the plant cell wall between two cells, lined by continguous plasma membrane and containing a central ER strand, and containing FG-NUP-based phase separation domains (position tentative).

Main text

The exchange of nutrients and intercellular communication between cells is essential for the efficient functioning of multicellular organisms. In addition to exchange across the intercellular space via transporters and receptors, metazoa, fungi and plants have all independently evolved direct cell-cell bridges. The green lineage developed unique structures, called plasmodesmata (PD), which are composed of modified cell wall domains that are traversed by plasma membrane-lined channels that contain an ER-derived desmotubule and create continuity between the cytoplasm of neighboring cells. Since PD are embedded into the carbohydrate matrix of the cell walls and likely contain multiple membranes and soluble proteins, they pose a major challenge for biochemical and cell biological analyses. Several studies obtained PD proteomes by enriching membrane proteins in cell wall fractions (*7–10*). Genetic approaches have so far failed to help identify genes that could fully explain the transport mechanism, possibly due to redundancy or lethality of the mutants. Transport studies have been challenging since intact multicellular systems are required for analyses.

Key features of PD transport appear to be the ability to translocate highly diverse cargo (from ions to macromolecules), a size exclusion limit (which, depending of the type of PD, can reach 70 kDa, in funnel PD even 120 kDa), and the ability to translocate specific cargo (*11*, *12*). Lee et al. highlighted that transport through PD and the nuclear pore complex (NPC) share common features (*13*). Both NPC and PD transport the same cargo species (ions, metabolites, proteins, and ribonucleoprotein complexes). For both NPC and PD, studies have described the ability for pore dilation (*14*, *15*). Both NPC and PD constitute selective barriers, allowing '*passive passage of molecules'* with a size exclusion limit (as used in animal literature; named '*non-targeted movement*' for PD) and '*facilitated translocation of specific macromolecules'* ('*targeted movement*' used in PD literature) (*16*, *17*). The core of the permeability barrier of the NPC appears to be a separated phase formed by disordered phenylalanine–glycine (FG) repeat-containing proteins, which function as 'smart sieves' (*17*). In a continuum, these smart sieves allow passage of smaller molecules and proteins without interaction with the FG repeats, while larger molecules or specific cargo pass with the help of nuclear transport receptors (NTR) that interact with the FG repeats (*18*).

As a shared structure among eukaryotes, the ultrastructure, function and transport mechanism of the NPC is well understood (*19*). The human NPC, with about 1000 polypeptides, has a diameter of 120 nm, a pore size of about 43 nm and a height of 80 nm and is composed of a membrane-anchor, three stacked rings (a sandwich of two outer and an inner ring), cytoplasmic filaments, and a nucleocytoplasmic basket (*20*). FG-nucleoporins (FG-NUPs), intrinsically disordered proteins containing FG repeat motifs produce phase-separated domains in a good Flory solvent-like environment *in situ* (*17*, *21–23*). Based on the above-mentioned common features shared between NPC and PD, we hypothesized that the PD transport mechanism could likewise contain FG-repeat proteins to generate a pore with similar properties as the NPC.

We first explored whether the green lineage may have evolved a distinct set of FG-repeat proteins. The human genome encodes twelve FG-NUPs: NUP42, NUP50, NUP54, NUP58 (aka NUP45), NUP62, NUP98, NUP153, NUP214, POM121, POM121B, POM121C, and NUP358 (*24*), while the Arabidopsis genome encodes ten FG-NUPs: NUP42 (aka CG1), NUP50a & NUP50b, NUP54, NUP58, NUP62, NUP98a & NUP98b, NUP136 and NUP214 (*25*, *26*). The majority of the FG-NUPs were conserved, with only three FG-NUPs not found in the green lineage (NUP153, POM121, NUP358). A bioinformatic search for FG repeat-containing proteins in the *Physcomitrium patens* genome found that 12 out of the 15 top-ranked FG-containing proteins were NUPs, while the other three proteins were not considered candidates for a transport function (table S1; file S1; file S2). Analysis of the subcellular localization of fluorescent protein (FP) fusions of three *P. patens* FG-NUPs (NUP58, NUP62 and NUP98) by confocal microscopy showed that all three protein signals overlaid in many cases the PD-associated callose dye (aniline blue) when transiently expressed in *N. benthamiana* (Fig. 1A; fig. S1). PD localization did not appear to be due to an FG-NUPs-specific mis-localization to PD, since the inner ring linker NUP35, which connects the transmembrane interaction hub with the ALADIN-NDC1 core to NUP155, also localized to PD (Fig. 1A). One might have speculated that the PD permeability barrier is generated by a set of NUPs that are derived by tandem gene duplications followed by differentiation into NPC and PD functions. However, previous phylogenetic analyses showed that the majority of NUPs are encoded by single genes,

refuting this hypothesis (table S2)(*26*, *27*). Independent evidence for PD localization of some NUPs stems from the identification of SEC13, FG-NUP50a, NUA in PD fractions of *P. patens* (*7*). Additionally, moss PD proteins are targeted to PD of tobacco leaves, indicating conservation of the targeting signals (*7*).

To obtain independent evidence and to explore whether vascular plant NUPs also show dual localization to NPC and PD, we utilized an established PD enrichment and data analysis pipeline to generate a PD proteome from Arabidopsis shoots (*7*). This approach, driven by the expanding knowledge of PD proteins, facilitates iterative identification of novel PD proteins. The resulting Arabidopsis shoot PD proteome has an 80% overlap with published PD proteomes and includes approximately 43% of the high-confidence PD proteins, including well established markers such as PDLPs and MCTPs (table S3, fig. S2, file S3)(*8*, *28*). Notably, a substantial number of Arabidopsis NUPs, specifically proteins from the inner and outer rings and the basket of the NPC, were found in the new high-confidence PD protein list (Fig. 1B). In total, 20 proteins covering different parts of the NPC were identified, and 15 were enriched in PD fractions compared to cell wall and total protein fractions from Arabidopsis (Fig. 1B, C, fig. S2). Several of the identified nuclear pore components passed the threshold for consideration as high-confidence PD proteins, in particular proteins of the inner and outer rings, core and basket. CPR5, GP210, NUP35, NUP93a, NUP155, NUP205, NUP43, HOS1 (aka HOS1/ELYS), SEC13, NUP62, NUP214, NUP50a, and NUP82 from Arabidopsis were also found in proteomics data of cell wall/PD protein fractions from others (table S4) (*7*, *9*, *10*, *29*, *30*).

To explore whether Arabidopsis NUPs can be detected at PD by confocal microscopy, candidates with C-terminal fluorescent protein fusions were expressed from an estradiol-inducible promoter in *N. benthamiana* leaves, which limits overexpression. Confocal imaging confirmed that the 15 tested NUP FP-fusions localized to the nucleus (fig. S3, list of 15 tested NUPs within table S2). Notably, 11 out of 15 NUPs localized to puncta in the cell periphery, and in many cases overlaid the aniline blue fluorescence (Fig. 2A, B; fig. S3)(*31*). These eleven NUPs showed a significant enrichment at PD when compared to a cell wall marker and/or cytoplasmic control (Fig. 2B). Among them were two FG-NUPs (NUP62 and NUP98b), two outer ring NUPs (NUP43, HOS1/ELYS), and two transmembrane NUPs (GP210, CPR5) (Fig. 1C, 2B). Aniline blue stains callose (β-1,3-glucan), which is deposited at the neck region of PD. In case the callose deposition is low, PD might not be stained by aniline blue, which is why we did not expect a 100% overlay. Since, as in other studies, the overlay of PD proteins with aniline blue was not 100%, the overlay of the *bona fide* PD protein PDLP5 was evaluated. Consistent with the above, PD targeting of the putative NUP107-160 complex recruitment factor HOS1/ELYS as an mCitrine fusion showed overlay with both aniline blue fluorescence as well as the PD marker PDLP5-mScarlet3 at PD (Fig. 2C).

To evaluate whether the PD localization was an artifact caused by overexpression, estradiol concentration and induction time were reduced, leading to reduced overall fluorescence intensity, however without affecting the localization to both NPC and PD (Fig. 2D). Analysis of stably transformed Arabidopsis lines expressing a GFP gene fused in front of the stop codon of a full-length genomic *FG-NUP62* gene also showed localization to both nuclei and PD in cotyledons, making an artifact rather unlikely (Fig. 2E, fig. S4). As Arabidopsis FG-NUP62 was previously shown to form hydrogels that recapitulate the NPCs phase separation-like transport properties *in vitro*, localization of FG-NUP62-GFP at PD in a stably transformed Arabidopsis line is in line with the idea of a phase separation as permeability barrier at PD(*32*).

Notably, and in contrast to C-terminal FP fusions of the auto-cleavable NUP98a (*33*), a C-terminal NUP98b-mVenus fusion produced fluorescence and efficiently localized to PD (Fig. 2), indicating that either the main fraction of NUP98b in the previous study was unprocessed, or that the C-terminal peptide reassociated with the N-terminal domain of NUP98b, as previously described for the two splice forms of human NUP98 (*34*). Out of the 15 tested NUPs, four NUPs did not localize at PD, as indicated by *p*-values greater than 0.08 (table S2). Out of the 35 currently known Arabidopsis NUPs, 20 NUPs were not tested here (table S2). In summary, our data indicate that NUPs of the non-vascular moss *P. patens* and the vascular plant Arabidopsis are present both at the NPC and PD, including the plant-specific membrane anchor CPR5 and FG-NUP NUP62. Components of the inner ring, NUP93a and NUP155, and the basket, NUP82, were also detected at PD, although with lower confidence as compared to, e.g., CPR5. Analysis of published data from other groups who had localized a variety of NUPs to nuclei also showed peripheral puncta, which had not previously been analyzed further (table S5). Our proteomics and localization data are consistent with dual targeting of NUPs and with the existence of a plasmodesmatal pore complex

(PDPC). While it is conceivable that NUPs may contain distinct NPC and PD targeting sequences, an alternative hypothesis might be that they are recruited to the two locations by a common receptor or anchor, where they assemble a pore that harbors a phase separation and constitute a permeability barrier.

Four potential membrane proteins that anchor the NPC in the nuclear membrane had been identified in the human genome: GP210, POM121, NDC1 and TMEM33. Arabidopsis encodes genes for three conserved membrane anchor homologs, namely GP210, NDC1 and TMEM, plus the green lineage-specific CPR5 (table S6). CPR5 has been proposed to serve as an anchor in the equatorial plane of the NPC (*35*)(fig. S5). Since CPR5 was among the top 5 candidates based on the PD index, it might also serve as an anchor of an NPC-like structure at PD (Fig. 2A, B). CPR5, a polytopic membrane protein, is predicted to form a globular helix bundle domain at its cytosolic N-terminus, that is flanked by disordered regions and connected to a 105 amino acid central α-helix (fig. S5). The central helix contains a hydrophobic region which, together with 4 shorter hydrophobic helices, forms an approximately 35 Å long transmembrane domain, which is consistent with the expected thickness of ER membranes, while its C-terminus extends into the ER lumen. CPR5 may thus serve as a replacement for the missing metazoan POM121 (*36*). CPR5 is encoded by a single gene in Arabidopsis and by two in the monocot *Oryza sativa* (*37*)(fig. S6, table S6, table S7).

Principal differences between the NPC and PD are the overall length (nuclear membrane thickness at the pore ～30 nm, PD, depends on cell wall thickness, between 100 nm and several μm), the presence of a nuclear double-membrane *vs*. two separate membranes at PD, an outer plasma membrane and an ER-like desmotubule membrane, and the presence of the desmotubule as a tubular structure in the center of the pore. We surmise that the PDPC must be arranged in a different manner, either extending from the plasma membrane or the desmotubule, and either positioned at the orifices or located inside the channel. Although cryoET structures of plant NPCs are not available (unlike human NPC), it has been suggested that CPR5 is likely embedded into the ER-type nuclear membrane at the equatorial plane (*35*). In PD, CPR5 could either be embedded into the PD plasma membrane, with the C-terminus facing the apoplasm, or be embedded into the ER/desmotubule membrane, with the C-terminus facing the ER/desmotubule lumen and the long N-terminal domain pointing into the intermembrane space in PD, analogous to the CPR5 toplogy in the ER-derived nuclear membrane at the NPC. A split-GFP system for topology studies of membrane proteins was used to determine whether the C-terminus of CPR5 faces the luminal side of the ER (*38*). When GFP11-CPR5 was co-expressed with cytosolic GFP1-10, but not a GFP1-10 targeted to the ER lumen, fluorescence was reconstituted (Fig. 3A, B; fig. S7). The complementary fusion of CPR5-GFP11 led to reconstituted fluorescence when co-expressed with a GFP1-10 domain targeted and retained in the ER lumen (GFP1-10-HDEL), but not with GFP1-10 co-expressed in the cytosol (Fig. 3A, B; fig. S7). The topological data are consistent with a model in which the C-terminal five-helix-bundle of CPR5 traverses the ER/desmotubule membrane with the C-terminus inside the lumen of the ER/desmotubule, while the extended central α-helix, the predicted unstructured domains, and the smaller helical bundle of CPR5 is located in the intermembrane space between the ER/desmotubule and the plasma membrane. When fully extended, the unstructured domains should be able to span the whole space between the ER and the plasma membrane within the PD, possibly serving as part of an anchor for the NUP complexes in the intermembrane space of the PD (fig. S5).

If we assume that NUPs are anchored on the desmotubule extending into the cytoplasmic channel, the question arises where in PD such a structure is located, e.g., either as a barrier in the central cavity or at the orifices. Structured illumination microscopy (SIM) was used to determine the localization at PD at higher resolution using CPR5 fused to mCitrine. CPR5 localized to the neck region of the pore adjacent to aniline blue labeled callose deposition (Fig. 3C, D; fig. S8), but not in the central cavity of the pore, where PDLP5-mScarlet3 was localized (*39*). This finding is consistent with a model in which NPC-like pores are present at the orifices. We did not observe puncta at both paired neck regions across cells in all cases (fig. 8B, top), which may be due to either the mosaic-like expression in *N. benthamiana*, in which only one of the adjacent cells expressed the fusion protein, or an asymmetry of different PD that might have a barrier only on one side of the PD (for Model with barrier on both sides, see Fig. 3D).

If NUPs form NPC-like pores at PD that are involved in the control of cell-to-cell transport, one may expect that interfering with NUP function will lead to changed cell-to-cell transport of cargo such as proteins. To test this *in vivo*, we obtained two different *cpr5* loss-of-function mutant plants, the EMS

mutant *cpr5-1* (G420D) and the T-DNA insertion mutant *cpr5-T3* (*40*, *41*). Both mutants were severely dwarfed (fig. S9C, D). The *cpr5* phenotypes may be caused by defects in NPC or PD functions, or both (*35*, *42*). To test whether loss-of-function mutations of CPR5 impact the cell-to-cell translocation of proteins, we transiently expressed a tandem-GFP fusion (2xmEGFP; 54 kDa) by particle bombardment of Arabidopsis leaves (*43–45*). While 2xmEGFP signals spread cell-to-cell in WT-Col-0, there was a significant reduction of 2xmEGFP spread in *cpr5-1* and *cpr5-T3*, indicating that the plasmodesmatal-mediated cell-to-cell diffusion was decreased (Fig. 4A, B; fig. S9A). Originally named for its *constitutive pathogen response* phenotype, loss of CPR5 activity can trigger constitutive defense responses that trigger callose deposition and possibly closure of PD (*46*). Callose levels were quantified and compared between wild-type and *cpr5-1* Arabidopsis leaves, but no significant differences were found (Fig. 4C), indicating that an increase in callose deposition did not lead to a defect in cell-to-cell GFP diffusion. GFP transport through PD is characterized by a low activation energy, indicating passive diffusion rather than energy-dependent mechanisms as needed for facilitated transport (*47*). Together, our data are consistent with a role of CPR5 in the diffusion-based transport through PD of proteins sized below the exclusion limit, possibly as a membrane anchor.

If CPR5 serves as an important component of PD, one might expect that not only diffusion of large proteins but also facilitated (targeted) translocation of, e.g., transcription factors, is negatively impacted in *cpr5* loss-of-function mutants. The non-cell-autonomous transcription factor SHORT-ROOT (SHR) is expressed in the stele and is transported cell-to-cell into the endodermis followed by nuclear import (*48*). Cell-to-cell transport of SHR is crucial for tissue patterning and thus plant development (*48–50*). To investigate whether targeted cell-to-cell transport of SHR-GFP (86.6 kDa) was also impacted in a *cpr5* loss-of-function mutant, we quantified the endodermis-to-stele ratio (E:S ratio) of GFP fluorescence in roots of *shr*/pSHR:SHR–GFP/WT and *shr*/pSHR:SHR–GFP/*cpr5-1* lines. The E:S ratio was significantly reduced in *cpr5-1* compared to WT background, consistent with the hypothesis that facilitated transport across PD is also reduced in the *cpr5-1* mutant (Fig. 4D, E). Alternatively, changes in E:S ratio might also result from a changed protein biosynthesis of SHR-GFP in the *cpr5-1* mutant background. We therefore compared also GFP fluorescence in the stele of *shr*/pSHR:SHR–GFP/WT and *shr*/pSHR:SHR–GFP/*cpr5-1* lines and could not find a significantly different fluorescence intensity (fig. S9E), ruling out changed protein biosynthesis of SHR-GFP in the *cpr5* mutant background. If a phase separation in an NPC-like pore constitutes the selectivity barrier at PD, we would expect transport changes in NUP mutant lines for macromolecules -as reported here- rather than for a small molecule dye. To better understand the cause of the transport changes in the *cpr5* mutant lines, we performed the DropANd See diffusion assay (DANS) (Fig. 4F-H), using the small molecule dye 5-(and-6)-carboxyfluorescein diacetate/ succinimidyl ester CFDA/CFSE which is cleaved by cytosolic esterases to 5-(and-6)-carboxyfluorescein CF (MW 376 Da), that is commonly used to assess symplasmic diffusion. We quantified the diffusion of CF in Arabidopsis leaves and compared NUP *cpr5* and *nup62* mutant lines with WT and *35S:PDLP5* overexpression line (Fig. 4I). Neither *cpr5* mutant lines nor FG-NUP *nup62* mutant lines showed decreased symplasmic diffusion compared to WT (Fig. 4I). By contrast, in the *35S:PDLP5* overexpression line, which previously has been shown to have increased callose deposition at PD resulting in lower PD permeabilities, the diffusion was significantly decreased (Fig. 4I)(*51*). The specificity of the changes in transport of macromolecules in the *cpr5* mutant background is further in line with the idea of a phase separation as permeability barrier at PD. Transport for macromolecules might be changed in the *cpr5* mutant background due to insufficient anchoring of the PDPC, which might result in an altered organization and therefore different transport features of the PDPCs phase-separating FG-mesh. Of note, if changed PD density/distribution (i.e. lower abundance) or changed morphology (e.g. increased callose deposition at neck regions) in the *cpr5* mutant background is the predominant reason for the observed transport changes for macromolecules, the symplasmic diffusion of the small molecule dye CF in the DANS assay should have been changed as well. The changes in transport through PD observed here are size specific which suggests a change of internal PDPC gating rather than changes in PD distribution, state, or morphology.

Based on the presence of FG-NUPs in the PDPC, facilitated transport might involve similar mechanisms as in the NPC (*18*). One may speculate that some aspects of the observed defects of the Arabidopsis *cpr5* mutants, such as growth deficiency or pathogen resistance (fig. S9C, D), may be caused by defects in both nuclear and PD transport. The defects in both diffusive and targeted intercellular transport are in line with the presence of a pore complex at the orifices of PD with similar components as the NPC. This PDPC

could be involved in mediating cell-to-cell diffusion and transport through PD. 11 out of the 15 known plant NUPs tested here showed a significant enrichment at PD. Both the exact composition and structure of the predicted PDPC and how dual targeting is achieved remains to be explored. Not all NUPs present in the NPC have been tested here, and not all NUPs tested here were found to be present in PD (table S2). Whether these NUPs are indeed not present in the PDPC or we did not detect them will require additional experiments.

Notably, the import of proteins into primary cilia at the transition zone also shares similarities with nuclear transport (*52*). Multiple NUPs, including the cytoplasmic FG-NUP214, the outer ring NUP37 and NUP85, the inner ring NUP35 and NUP188, the linker NUP93, and the central FG-NUP62 and NUP98 localize to the ciliary base. A series of elegant experiments aimed at inhibiting the activity of NUPs at primary cilia provided evidence for a role in protein import into cilia (*53*) and potentially another example for NUPs being recruited to form a pore outside of the nucleus.

Here we provide evidence for NUPs to also localize to PD, forming a PDPC. The presence of FG-NUPs at PD suggests the presence of a phase separation as permeability barrier in the PDPC. Interfering with NUP function changes transport for macromolecules but not for a small molecule dye, which is in line with the idea of a phase separation as permeability barrier at PD. This work may open new ways to understand the structure, function, transport mechanism and regulation of PD and how to engineer the permeability barrier between cells.

References

1. E. Tangl, Über offene Kommunikationen zwischen den Zellen des Endosperms einiger Samen. *Jahrb. Für Wiss. Bot.* **12**, 170–190 (1879).
2. E. Strasburger, Über Plasmaverbindungen pflanzlicher Zellen. *Jahrb. Für Wiss. Bot.* **36**, 493–610 (1901).
3. J. A. Raven, "Evolution of Plasmodesmata" in *Plasmodesmata* (John Wiley & Sons, Ltd, 2007; https://onlinelibrary.wiley.com/doi/abs/10.1002/9780470988572.ch2), pp. 33–52.
4. M. Miras, M. Pottier, T. M. Schladt, J. O. Ejike, L. Redzich, W. B. Frommer, J.-Y. Kim, Plasmodesmata and their role in assimilate translocation. *J. Plant Physiol.* **270**, 153633 (2022).
5. W. S. Peters, K. H. Jensen, H. A. Stone, M. Knoblauch, Plasmodesmata and the problems with size: Interpreting the confusion. *J. Plant Physiol.* **257**, 153341 (2021).
6. W. J. Nicolas, M. S. Grison, E. M. Bayer, Shaping intercellular channels of plasmodesmata: the structure-to-function missing link. *J. Exp. Bot.* **69**, 91–103 (2017).
7. S. Gombos, M. Miras, V. Howe, L. Xi, M. Pottier, N. S. Kazemein Jasemi, M. Schladt, J. O. Ejike, U. Neumann, S. Hänsch, F. Kuttig, Z. Zhang, M. Dickmanns, P. Xu, T. Stefan, W. Baumeister, W. B. Frommer, R. Simon, W. X. Schulze, A high-confidence *Physcomitrium patens* plasmodesmata proteome by iterative scoring and validation reveals diversification of cell wall proteins during evolution. *New Phytol.* **238**, 637–653 (2023).
8. M. L. Brault, J. D. Petit, F. Immel, W. J. Nicolas, M. Glavier, L. Brocard, A. Gaston, M. Fouché, T. J. Hawkins, J.-M. Crowet, M. S. Grison, V. Germain, M. Rocher, M. Kraner, V. Alva, S. Claverol, A. Paterlini, Y. Helariutta, M. Deleu, L. Lins, J. Tilsner, E. M. Bayer, Multiple C2 domains and transmembrane region proteins (MCTPs) tether membranes at plasmodesmata. *EMBO Rep.* **20**, e47182 (2019).
9. L. Fernandez-Calvino, C. Faulkner, J. Walshaw, G. Saalbach, E. M. Bayer, Y. Benitez-Alfonso, A. J. Maule, Arabidopsis plasmodesmal proteome. *PloS One* **6**, e18880 (2011).
10. E. M. Bayer, A. R. Bottrill, J. Walshaw, M. Vigouroux, M. J. Naldrett, C. L. Thomas, A. J. Maule, Arabidopsis cell wall proteome defined using multidimensional protein identification technology. *PROTEOMICS* **6**, 301–311 (2006).

11. D. S. G. Paultre, M.-P. Gustin, A. Molnar, K. J. Oparka, Lost in transit: long-distance trafficking and phloem unloading of protein signals in Arabidopsis homografts. *Plant Cell* **28**, 2016–2025 (2016).

12. T. J. Ross-Elliott, K. H. Jensen, K. S. Haaning, B. M. Wager, J. Knoblauch, A. H. Howell, D. L. Mullendore, A. G. Monteith, D. Paultre, D. Yan, S. Otero, M. Bourdon, R. Sager, J.-Y. Lee, Y. Helariutta, M. Knoblauch, K. J. Oparka, Phloem unloading in Arabidopsis roots is convective and regulated by the phloem-pole pericycle. *eLife* **6**, e24125 (2017).

13. J. Y. Lee, B. C. Yoo, W. J. Lucas, Parallels between nuclear-pore and plasmodesmal trafficking of information molecules. *Planta* **210**, 177–187 (2000).

14. C. E. Zimmerli, M. Allegretti, V. Rantos, S. K. Goetz, A. Obarska-Kosinska, I. Zagoriy, A. Halavatyi, G. Hummer, J. Mahamid, J. Kosinski, M. Beck, Nuclear pores dilate and constrict in cellulo. *Science* **374**, eabd9776 (2021).

15. F. Kragler, J. Monzer, K. Shash, B. Xoconostle-Cázares, W. J. Lucas, Cell-to-cell transport of proteins: requirement for unfolding and characterization of binding to a putative plasmodesmal receptor. *Plant J.* **15**, 367–381 (1998).

16. K. M. Crawford, P. C. Zambryski, Non-targeted and targeted protein movement through plasmodesmata in leaves in different developmental and physiological states. *Plant Physiol.* **125**, 1802–1812 (2001).

17. S. Frey, R. Rees, J. Schünemann, S. C. Ng, K. Fünfgeld, T. Huyton, D. Görlich, Surface properties determining passage rates of proteins through nuclear pores. *Cell* **174**, 202-217.e9 (2018).

18. R. H. Kehlenbach, P. Neumann, R. Ficner, A. Dickmanns, Interaction of nucleoporins with nuclear transport receptors: a structural perspective. *Biol. Chem.* **404**, 791–805 (2023).

19. S. Mosalaganti, A. Obarska-Kosinska, M. Siggel, R. Taniguchi, B. Turoňová, C. E. Zimmerli, K. Buczak, F. H. Schmidt, E. Margiotta, M.-T. Mackmull, W. J. H. Hagen, G. Hummer, J. Kosinski, M. Beck, AI-based structure prediction empowers integrative structural analysis of human nuclear pores. *Science* **376**, eabm9506 (2022).

20. D. H. Lin, A. Hoelz, The structure of the nuclear pore complex (an update). *Annu. Rev. Biochem.* **88**, 725–783 (2019).

21. S. C. Ng, T. Güttler, D. Görlich, Recapitulation of selective nuclear import and export with a perfectly repeated 12mer GLFG peptide. *Nat. Commun.* **12**, 4047 (2021).

22. B. W. Hoogenboom, L. E. Hough, E. A. Lemke, R. Y. H. Lim, P. R. Onck, A. Zilman, Physics of the nuclear pore complex: Theory, modeling and experiment. *Phys. Rep.* **921**, 1–53 (2021).

23. M. Yu, M. Heidari, S. Mikhaleva, P. S. Tan, S. Mingu, H. Ruan, C. D. Reinkemeier, A. Obarska-Kosinska, M. Siggel, M. Beck, G. Hummer, E. A. Lemke, Visualizing the disordered nuclear transport machinery in situ. *Nature* **617**, 162–169 (2023).

24. L. J. Terry, S. R. Wente, Flexible gates: dynamic topologies and functions for FG nucleoporins in nucleocytoplasmic transport. *Eukaryot. Cell* **8**, 1814–1827 (2009).

25. K. Chopra, S. Bawaria, R. Chauhan, Evolutionary divergence of the nuclear pore complex from fungi to metazoans. *Protein Sci.* **28**, 571–586 (2019).

26. A. A. Makarov, N. E. Padilla-Mejia, M. C. Field, Evolution and diversification of the nuclear pore complex. *Biochem. Soc. Trans.* **49**, 1601–1619 (2021).

27. C. Zhang, N. An, P. Jia, W. Zhang, J. Liang, X. Zhang, H. Zhou, W. Ma, M. Han, L. Xing, X. Ren, Genomic identification and expression analysis of nuclear pore proteins in *Malus domestica*. *Sci. Rep.* **10**, 17426 (2020).

28. C. L. Thomas, E. M. Bayer, C. Ritzenthaler, L. Fernandez-Calvino, A. J. Maule, Specific targeting of a plasmodesmal protein affecting cell-to-cell communication. *PLoS Biol.* **6**, e7 (2008).

29. M. E. Kraner, C. Müller, U. Sonnewald, Comparative proteomic profiling of the choline transporter-like1 (CHER1) mutant provides insights into plasmodesmata composition of fully developed *Arabidopsis thaliana* leaves. *Plant J. Cell Mol. Biol.* **92**, 696–709 (2017).

30. P. Kirk, S. Amsbury, L. German, R. Gaudioso-Pedraza, Y. Benitez-Alfonso, A comparative meta-proteomic pipeline for the identification of plasmodesmata proteins and regulatory conditions in diverse plant species. *BMC Biol.* **20**, 128 (2022).

31. R. Zavaliev, B. L. Epel, Imaging callose at plasmodesmata using aniline blue: quantitative confocal microscopy. *Methods Mol. Biol. Clifton NJ* **1217**, 105–119 (2015).

32. J. Wang, G. Pei, Y. Wang, D. Wu, X. Liu, G. Li, J. He, X. Zhang, X. Shan, P. Li, D. Xie, Phase separation of the nuclear pore complex facilitates selective nuclear transport to regulate plant defense against pathogen and pest invasion. *Mol. Plant* **16**, 1016–1030 (2023).

33. M. Gallemí, A. Galstyan, S. Paulišić, C. Then, A. Ferrández-Ayela, L. Lorenzo-Orts, I. Roig-Villanova, X. Wang, J. L. Micol, M. R. Ponce, P. F. Devlin, J. F. Martínez-García, DRACULA2 is a dynamic nucleoporin with a role in regulating the shade avoidance syndrome in Arabidopsis. *Development* **143**, 1623–1631 (2016).

34. A. E. Hodel, M. R. Hodel, E. R. Griffis, K. A. Hennig, G. A. Ratner, S. Xu, M. A. Powers, The three-dimensional structure of the autoproteolytic, nuclear pore-targeting domain of the human nucleoporin Nup98. *Mol. Cell* **10**, 347–358 (2002).

35. Y. Gu, S. G. Zebell, Z. Liang, S. Wang, B.-H. Kang, X. Dong, Nuclear pore permeabilization is a convergent signaling event in effector-triggered immunity. *Cell* **166**, 1526-1538.e11 (2016).

36. L. Apelt, K. E. Knockenhauer, N. C. Leksa, N. Benlasfer, T. U. Schwartz, U. Stelzl, Systematic protein–protein interaction analysis reveals intersubcomplex contacts in the Nuclear Pore Complex. *Mol. Cell. Proteomics MCP* **15**, 2594–2606 (2016).

37. Y. Arra, F. Auguy, M. Stiebner, S. Chéron, M. M. Wudick, M. Miras, V. Schepler-Luu, S. Köhler, S. Cunnac, W. B. Frommer, L. Albar, Rice Yellow Mottle Virus resistance by genome editing of the *Oryza sativa L. ssp. japonica* nucleoporin gene *OsCPR5.1* but not *OsCPR5.2*. *Plant Biotechnol. J.* **22**, 1299–1311 (2024).

38. W. Xie, M. E. Nielsen, C. Pedersen, H. Thordal-Christensen, A split-GFP gateway cloning system for topology analyses of membrane proteins in plants. *PLOS ONE* **12**, e0170118 (2017).

39. J. Fitzgibbon, K. Bell, E. King, K. Oparka, Super-resolution imaging of plasmodesmata using three-dimensional structured illumination microscopy. *Plant Physiol.* **153**, 1453–63 (2010).

40. F. Wang, L. Wang, L. Qiao, J. Chen, M. B. Pappa, H. Pei, T. Zhang, C. Chang, C.-H. Dong, Arabidopsis CPR5 regulates ethylene signaling via molecular association with the ETR1 receptor. *J. Integr. Plant Biol.* **59**, 810–824 (2017).

41. S. A. Bowling, J. D. Clarke, Y. Liu, D. F. Klessig, X. Dong, The cpr5 mutant of Arabidopsis expresses both NPR1-dependent and NPR1-independent resistance. *Plant Cell* **9**, 1573–84 (1997).

42. S. Otero, Y. Helariutta, Y. Benitez-Alfonso, Symplastic communication in organ formation and tissue patterning. *Curr. Opin. Plant Biol.* **29**, 21–28 (2016).

43. K. M. Crawford, P. C. Zambryski, Subcellular localization determines the availability of non-targeted proteins to plasmodesmatal transport. *Curr. Biol.* **10**, 1032–1040 (2000).

44. C. Faulkner, E. Petutschnig, Y. Benitez-Alfonso, M. Beck, S. Robatzek, V. Lipka, A. J. Maule, LYM2-dependent chitin perception limits molecular flux via plasmodesmata. *Proc. Natl. Acad. Sci.* **110**, 9166–9170 (2013).

45. W. Sakulkoo, M. Osés-Ruiz, E. Oliveira Garcia, D. M. Soanes, G. R. Littlejohn, C. Hacker, A. Correia, B. Valent, N. J. Talbot, A single fungal MAP kinase controls plant cell-to-cell invasion by the rice blast fungus. *Science* **359**, 1399–1403 (2018).

46. A. Kohler, S. Schwindling, U. Conrath, Benzothiadiazole-induced priming for potentiated responses to pathogen infection, wounding, and infiltration of water into leaves requires the *NPR1/NIM1* gene in Arabidopsis. *Plant Physiol.* **128**, 1046–1056 (2002).

47. G. Schönknecht, J. E. Brown, J. Verchot-Lubicz, Plasmodesmata transport of GFP alone or fused to potato virus X TGBp1 is diffusion driven. *Protoplasma* **232**, 143–152 (2008).

48. K. Nakajima, G. Sena, T. Nawy, P. N. Benfey, Intercellular movement of the putative transcription factor SHR in root patterning. *Nature* **413**, 307–311 (2001).

49. K. Koizumi, T. Hayashi, S. Wu, K. L. Gallagher, The SHORT-ROOT protein acts as a mobile, dose-dependent signal in patterning the ground tissue. *Proc. Natl. Acad. Sci. U. S. A.* **109**, 13010–13015 (2012).

50. C. M. Winter, P. Szekely, V. Popov, H. Belcher, R. Carter, M. Jones, S. E. Fraser, T. V. Truong, P. N. Benfey, SHR and SCR coordinate root patterning and growth early in the cell cycle. *Nature*, 1–6 (2024).

51. J.-Y. Lee, X. Wang, W. Cui, R. Sager, S. Modla, K. Czymmek, B. Zybaliov, K. van Wijk, C. Zhang, H. Lu, V. Lakshmanan, A plasmodesmata-localized protein mediates crosstalk between cell-to-cell communication and innate immunity in Arabidopsis. *Plant Cell* **23**, 3353–3373 (2011).

52. H. Y. Chen, R. A. Kelley, T. Li, A. Swaroop, Primary cilia biogenesis and associated retinal ciliopathies. *Semin. Cell Dev. Biol.* **110**, 70–88 (2021).

53. C. A. Johnson, J. J. Malicki, The nuclear arsenal of cilia. *Dev. Cell* **49**, 161–170 (2019).

Acknowledgments

We would like to dedicate this manuscript to the 'champion of plasmodesmata', William J. (Bill) Lucas (UC Davis). We thank Gwen Davis for critical reading of the manuscript. We thank Madlen Somsich (HHU) for project coordination and management and Anita Snyder (www.anitaksnyder.com) for copyediting. This work has received funding from the European Research Council (ERC) and the Marie Skłodowska-Curie Actions under the European Union's Horizon 2020 research and innovation programme (Grant agreements 'SymPore' No. 951292 to WBF and "PDgate" No. 101023981 to MM, respectively). This research was also supported by the Deutsche Forschungsgemeinschaft (DFG, German Research Foundation) under Germany´s Excellence Strategy – EXC-2048/1 – project ID 390686111, and the Alexander von Humboldt Professorship, to WBF.

Data availability

Source data will be deposited at Dryad. Sequencing data for strains from this study have been deposited in the NCBI Sequence Read Archive (SRA) database under the accession codes will be provided at the time of publication. Materials will be made available under MTA; some materials were obtained from others as marked and require permission from the respective authors.

Contributions

WBF conceived of the study. J.E. performed the bioinformatic analyses; L.X., S.G. and W.S. performed proteomics and data analysis; M.D. analyzed the structure and generated fig. S4; S.H. helped to establish and advised on SIM. M.S, M.P., M.M., J.O.E., N.P., M.N., C.G. and A.D. performed imaging and transport studies; R.S. advised on imaging and data analyses; M.M. and A.R-E. performed split GFP studies, M.S, M.M., M.P., J.O.E., B.S., and W.B.F. analyzed the data; M.S., M.M., M.P., J.O.E., R.S. and W.B.F. wrote the manuscript.

Competing interests

We declare no competing interests.

Supplementary Materials

- Material and Methods
- 8 Supplementary Tables
- 10 Supplementary Figures
- 3 Supplementary files
- 2 Supplemental scripts
- Supplementary references

Figures and legends

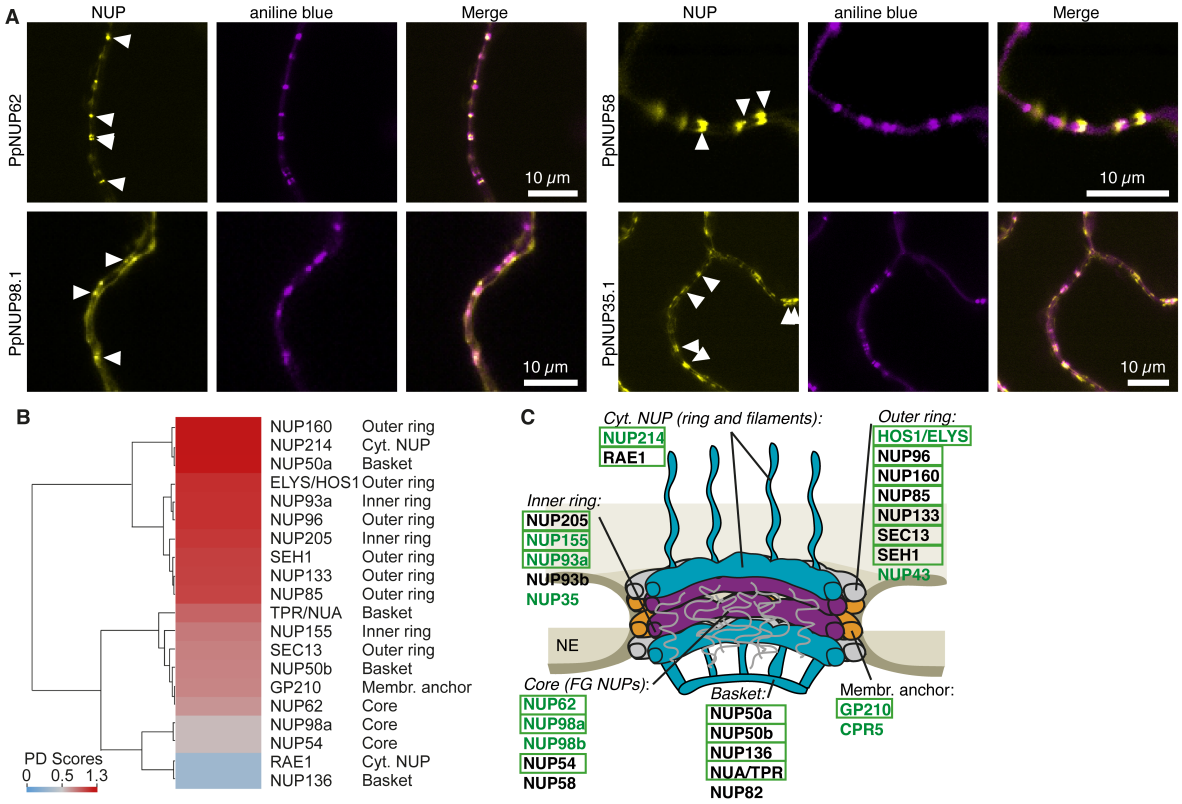

Figure 1. Identification of NUPs at plasmodesmata. (**A**) Localization of NUPs from *Physcomitrium patens* at PD. **(B)** Hierarchical clustering of PD scores of Arabidopsis NPC components found in PD proteome preparations from 5-week-old Arabidopsis shoot tissues. Clustering based on Euclidean distance of PD scores, which were averages of at least three replicate scores from separate tissue preparations. Color scale represents PD score values. PD scores above the high-confidence threshold of 0.5 are indicated in shades of red. **(C)** Scheme of an NPC embedded in the nuclear envelope with all NUPs studied in this work. NUPs listed in B are green boxed. NUPs found to be significantly enriched at PD in the transient localization assay (Fig. 2B) are written in green letters. Corresponding AGI locus identifiers in table S2. Cytoplasmic NUP is abbreviated as Cyt. NUP, and membrane anchor as Membr. anchor.

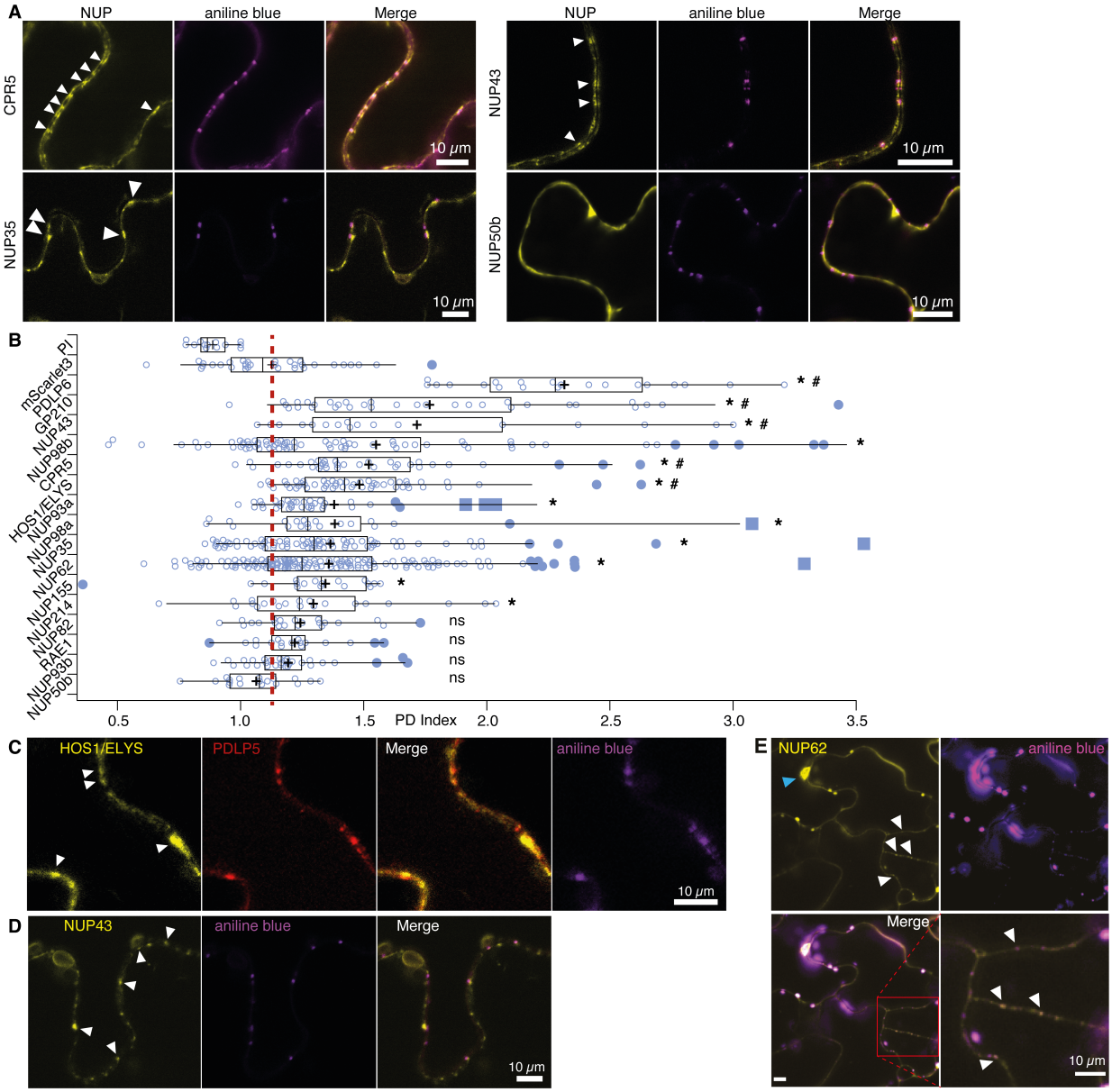

Figure 2. Analysis of the localization of Arabidopsis NUPs to PD. (A) Localization of selected Arabidopsis NUPs after transient expression under the control of the estradiol-inducible XVE promotor in *N. benthamiana* epidermal cells using confocal microscopy. mVenus was fused to the C-terminus of different NUPs, except for Nup98a for which GFP was fused both N- and C-terminally (GFP-NUP98a-GFP). Aniline blue was infiltrated to detect callose in pit fields as an indicator of plasmodesmata. Localization was repeated in three independent experiments with similar results. (**B**) Quantification of the PD localization by PD index. Red dashed line indicates the mean PD index of mScarlet3 (cytoplasmic control). PI, propidium iodide ('membrane impermeant dye'). Significantly ($p < 0.05$) increased PD indices compared to the cell wall or cytoplasmic controls are indicated by * and #, respectively. Kruskal-Wallis Test $p = <0.001$, p-values of Bonferroni corrected pairwise test are summarized in table S2. Median is represented by vertical line inside the box, mean is represented by the bold +. Values between quartiles 1 and 3 are represented by box ranges, and 5th and 95th percentile are represented by error bars. At least 15 images from 3 biological replicates were analyzed in each independent experiment. Independent localization data are shown in fig. S3. (**C**) Localization of HOS1/ELYS-mCitrine and PDLP5-mScarlet3 expressed transiently under the control of the inducible XVE promotor in *N. benthamiana* epidermal cells. Aniline blue was infiltrated to stain callose that accumulates in pit fields. The localization pattern has been repeated in three independent experiments with similar results. **(D)** NUP43-mCitrine localization at PD at 1/10 estradiol concentration and shortened induction time. **(E)** Localization of a genomic *NUP62* gene-

GFP fusion to nuclei (blue arow) and PD (white arrows) in cotyledons of stably transformed Arabidopsis lines. For the merged image a cropped and enlarged part of image is shown (bottom right, red box and lines). White arrowheads in A,D, and E indicate overlay of NUPs and aniline blue. White arrowheads in C indicate overlay of HOS1/ELYS-mCitrine and PDLP5-mScarlet3 channels.

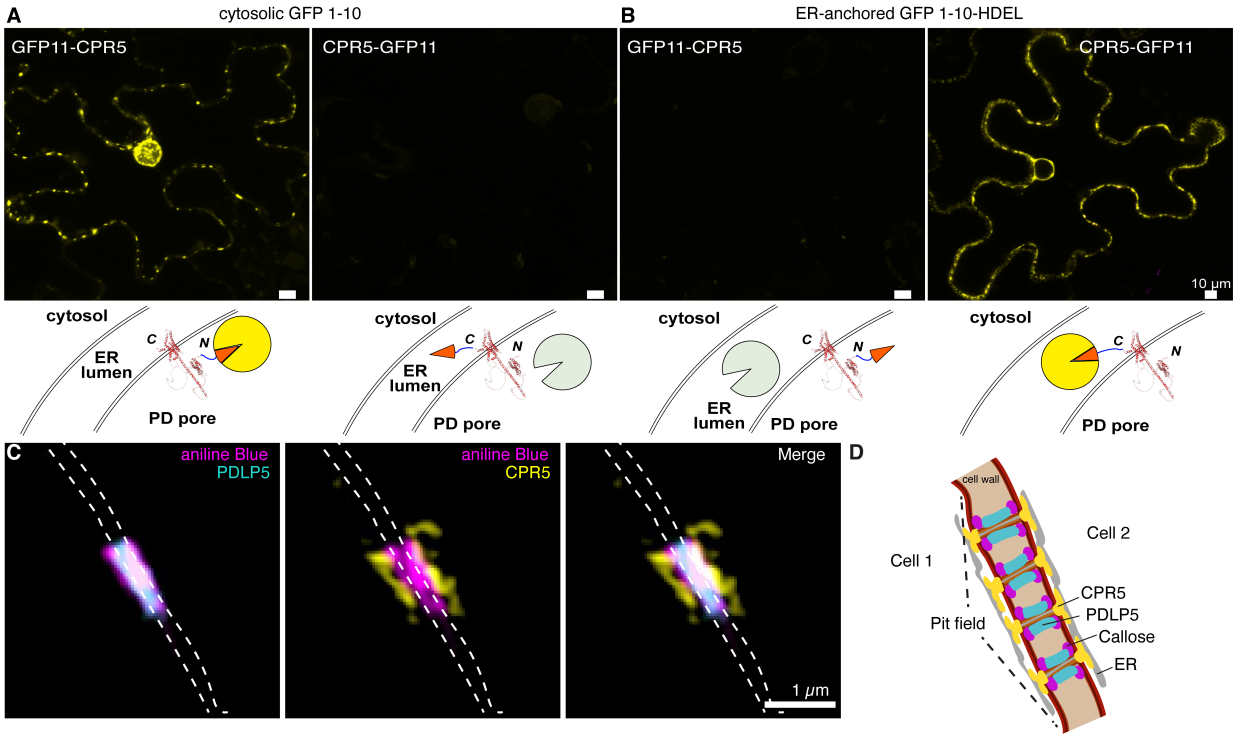

Figure 3. CPR5 topology and localization of CPR5 near PD orifices. Split-GFP membrane topology to test for the orientation of CPR5 in the nuclear pore membrane and the ER at PD. (**A**) *(left)* Fluorescence reconstitution at PD between a cytosolic non-fluorescent GFP domain lacking β-sheet 11 (GFP1-10; the circle missing a wedge) and a fusion of the GFP11 to the N-terminus of CPR5 (the red wedge). Since reconstitution occurs at PD, each cartoon indicates reconstitution in the intermembrane space between ER/desmotubule and plasma membrane. *(right)* Absence of fluorescence reconstitution between a cytosolic GFP1-10 and the fusion of the GFP11 to the C-terminus of CPR5. (**B**) *(left)* Absence of fluorescence reconstitution between an ER-retained GFP1-10-HDEL and a fusion of GFP11 to the N-terminus of CPR5. *(right)* Fluorescence reconstitution at PD between an ER-retained GFP1-10-HDEL and a fusion of the GFP11 to the C-terminus of CPR5. Repeated independently 3 times with comparable results. (**C**) Detection of CPR5-mCitrine close to the orifices of PD by Structured Illumination Microscopy (SIM) of *N. benthamiana* leaves co-infiltrated with XVE:PDLP5-mScarlet3 and XVE:CPR5-mCitrine. Prior to the imaging, leaves were infiltrated with aniline blue. PDLP5-mScarlet3 in turquoise, CPR5-mCitrine in yellow, and aniline blue in magenta. Repeated independently four times with comparable results. **(D)** Cartoon approximately to scale, illustrating plasmodesmata in a pitfield between two adjacent cells with callose marked in purple, PDLP5 in magenta and CPR5 in yellow.

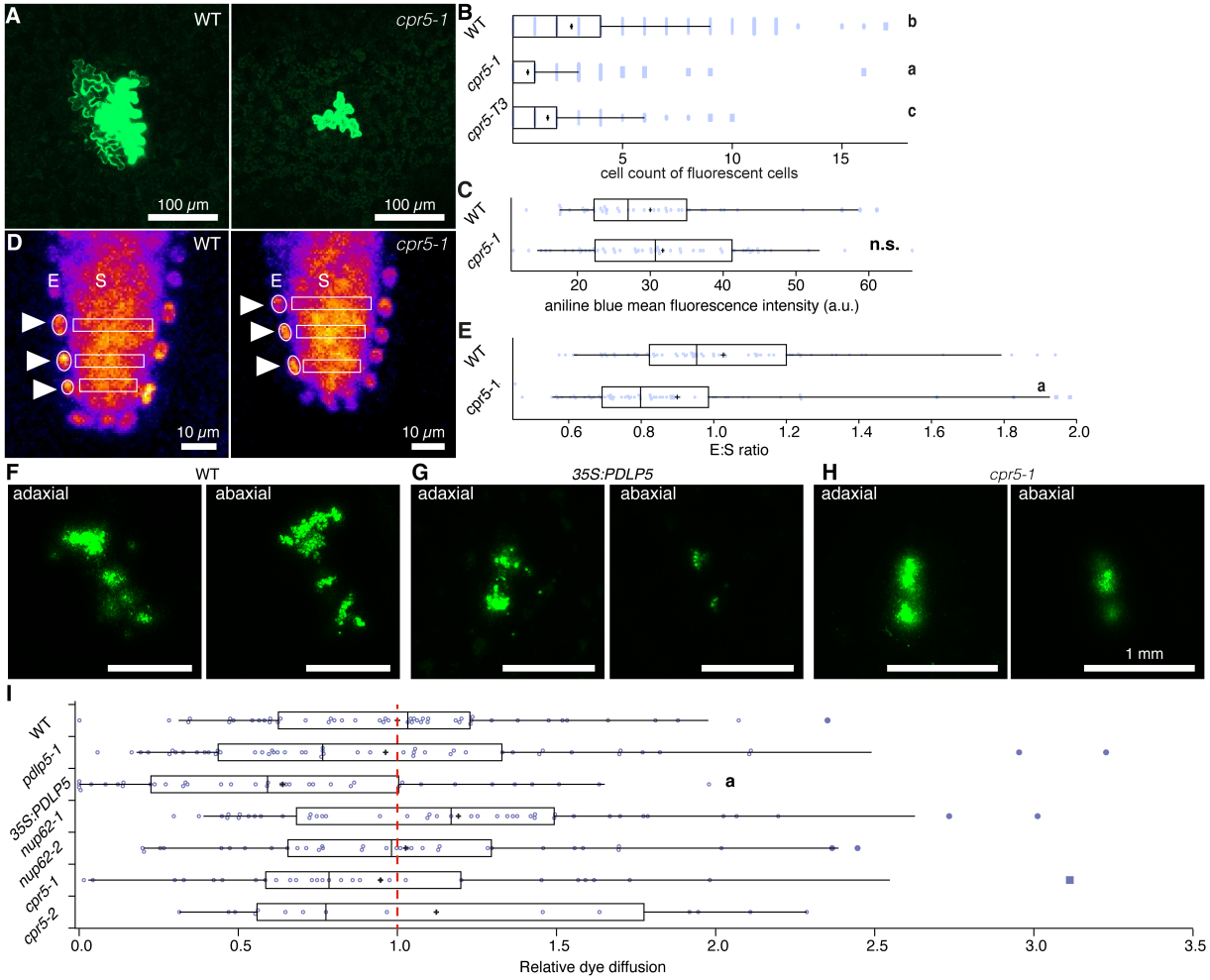

Figure 4. Defects in cell-to-cell transport of kDa-sized cargo in *cpr5* mutants. (A) Example images of intercellular 2xmEGFP movement in WT (*left*) and *cpr5-1* (*right*) Arabidopsis leaves. Leaves were bombarded with gold particles coated with p35S:mEGFP-mEGFP DNA plasmids 24 h prior to the experiment (fusion protein abbreviated as 2xmEGFP). **(B)** Quantification of the intercellular spread of mEGFP by counting fluorescent cells in the GFP channel. $n_{(WT)}$ = 594 bombarded cells, 17 independent biological replicates. $n_{(cpr5\text{-}1)}$ = 278 bombarded cells, 6 independent biological replicates. $n_{(cpr5\text{-}T3)}$ = 99 bombarded cells, 4 independent biological replicates. **a** indicates a significant difference to WT with $p_{(cpr5\text{-}T3)} = 0.0004$; **b** indicates a significant difference to WT with $p_{(cpr5\text{-}1)} < 10^{-15}$; $p_{(cpr5\text{-}1 \text{ vs. } cpr5\text{-}T3)} = 0.0002$ (Kruskal-Wallis test with Bonferroni correction for pairwise comparison). **(C)** Callose quantification. $n_{(WT)}$ = 4 independent experiments, $n_{(cpr5\text{-}1)}$ = 5 independent experiments, graph summarizes all experiments. Student´s *t*-test $p = 0.48$. **(D)** Sum projections showing SHR–GFP distribution in WT (*left*) and *cpr5-1* mutant (*right*) root. White circles and boxes indicate positions of endodermis nuclei (E, arrows) and corresponding regions in the stele (S, white boxes). **(E)** Quantification of SHR–GFP endodermis:stele ratio (E:S) for WT and *cpr5-1* mutant. $n_{(WT)}$ = 62 nuclei, $n_{(cpr5\text{-}1)}$ = 62 nuclei, with 3-4 nuclei analyzed per root. **a** indicates a significantly decreased E:S in *cpr5-1* mutant, based on Mann-Whitney U test with $p = 0.0006$. **(F-I)** PD permeabilities examined by CFDA/CFSE-based DANS dye loading assays. **(F-H)** Epifluorescence reporting on CF diffusion in the epidermis of the adaxial side (*left*) and abaxial (*right*) side of a leaf. WT (**F**), *35S:PDLP5* (**E**), and *cpr5-1* (**H**). Bars = 1 mm. **(I)** Quantification of CF diffusion in WT and mutant lines. $n_{(WT)}$ = 49 plants, 7 independent biological replicates; $n_{(pdlp5\text{-}1)}$ = 50 plants, 7 independent biological replicates; $n_{(35S:PDLP5)}$ = 38 plants, 6 independent biological replicates; $n_{(NUP62\text{-}1)}$ = 43 plants, 6 independent biological replicates; $n_{(NUP62\text{-}2)}$ = 34 plants, 5 independent biological replicates; $n_{(cpr5\text{-}1)}$ = 29 plants, 5 independent biological replicates; $n_{(cpr5\text{-}2)}$ = 15 plants, 5 independent biological replicates. The extent of dye diffusion was quantified by the ratio between the areal spread of fluorescence above a determined threshold on the abaxial side and the areal spread of

fluorescence above the same threshold on the adaxial side. **a** indicates significantly different at the $\alpha = 0.032$ level according to Bonferroni-corrected pair wise comparison following Kruskal-Wallis analysis.